Pool boiling heat transfer for surfaces with microchannels of variable depth

Robert Pastuszko[1*], *Milena* Bedla-Pawlusek[2] and *Robert* Kaniowski[1]

[1]Kielce University of Technology, Faculty of Mechatronics and Mechanical Engineering, al. 1000-lecia Państwa Polskiego 7, PL-25-314 Kielce, Poland
[2]Holy Cross Cancer Center, Technical Department, Artwińskiego Street 3, PL-25-734 Kielce

Abstract. Experimental investigations of pool boiling heat transfer on microchannels of variable depth were conducted. The experiments were carried out for water and ethanol at atmospheric pressure. Microchannels of variable depth from 0.2 to 2.8 mm and width 0.5 mm were uniformly spaced on base surface with pitch of 1 mm. The comparison of heat transfer coefficients for surfaces with variable and constant depth of microchannels was made. At the low and medium heat fluxes structures with constant microchannel depth showed the best boiling heat transfer performance. EX-FH20 (*Casio*) camera was used to record the images of the entire surface of the specimen. The bubble growth mechanism on the enhanced surface was different from that of plain surface. Visualization investigations were aimed at identifying nucleation sites and determining the bubble growth cycle. Vapor bubbles generate in microchannel spaces, from where they move towards the fin tips, then grow and depart.

1 Introduction

The paper deals with experimental investigations of boiling heat transfer on a system of parallel horizontal channels. This structures can be applied for cooling miniature integrated devices, such as microprocessors, by a direct or indirect method (as a thermosyphon or tube evaporator), substituting forced convection (traditional fan). An overview of the surfaces with microchannels and the heat transfer coefficients obtained are presented in Table 1.

Table 1. Types of open microchannels for pool boiling enhanced heat transfer

Reference	Configuration	Liquid	The highest HTC
Cooke and Kandlikar [1]	silicon micro-channels 40 – 200 μm wide and 180 – 275 μm deep, etched in silicon plates	water	73 kW/m^{2}K
Cooke and Kandlikar [2]	copper micro-channels 0.2 – 0.4 mm wide and 0.100 – 0.400 mm deep	water	269 kW/m^{2}K (channel width 0.375 mm, depth 0.4 mm)
Jaikumar and Kandlikar [3]	microchannels 300 μm, 500 μm and 762 μm wide, three coating configurations: sintered-throughout, sintered-fin-tops, sintered-channels.	water	2900 kW/m^{2}K, relative to the structured 10 x 10 mm^2 surface
Patil and Kandlikar [4]	microchannels (300—762 μm wide, 200—400 μm deep) with micro-porous coatings on the fin tops	water	995 kW/m^2 K for the 762 μm wide channel
Kalani and Kandlikar [5]	copper microchannels 245 – 470 μm deep and 194 – 406 μm wide	ethanol	72 kW/m^{2}K for 0.207 mm wide and 0.456 mm deep channel
Jaikumar and Kandlikar [6]	copper 762 μm wide and 400 μm deep open microchannel; coating configurations as in [4]	water	565 kW/m^{2}K
Jaikumar and Kandlikar [7]	copper open microchannels with porous fin tops on (widths: 300—762 μm, depths: 200—400 μm)	FC-87	20 kW/m^{2}K for the channel with the width and depth of 400 μm
Gheitaghy et al. [8]	copper surface on 45° inclined microchannels (widths: 0.5—0.7 mm, depths: 0.5—1 mm)	water	about 120 kW/m^{2}K for the channel width 0.5 mm and depth 1.4 mm
Kaniowski et al. [9]	microchannels 0.2—0.4 mm deep, 0.3 mm wide	water Novec-649	about 64 kW/m^{2}K (water) and 8 kW/m^{2}K (Novec-649)
Kaniowski and Pastuszko [10]	copper microchannels 0.3 mm wide, 0.2—0.5 mm deep	water ethanol FC-72	63 kW/m^{2}K (water), 20 kW/m^{2}K (ethanol)

* Corresponding author: tmprp@tu.kielce.pl

Kaniowski and Pastuszko [11]	copper microchannels 0.3 mm wide, 0.2—0.5 mm deep	ethanol FC-72	exceeded 20 kW/m^{2}K for ethanol and 10 kW/m^{2}K for FC-72
Kalani and Kandlikar [12]	copper open microchannels (widths: 194—406 μm, depths: 245—470 μm), 16.7—101.3 kPa	ethanol	about 65 kW/m^{2}K for the channel width 0.2 mm and depth 0.456 mm (at 101.3 kPa)
Rahman and McCarthy [13]	copper microchannel (characteristic lengths of 300μm to 3mm) with nanostructured coatings (characteristic lengths of 50 nm to 50μm)	water	461 kW/m^2 K
Kwak et al. [14]	copper microchannel with SiO_2 layer (widths: 30 μm, depths: 10—100 μm)	water	about 60 kW/m^{2}K for the channel width 30 μm, depths 100 μm
Walunj and Sathyabhama [15]	rectangular, parabolic and stepped microchannels on 10-mm diameter copper rod; channel widths: 250—800 μm; depth: 500 μm.	water	about 16 kW/m^{2}K

The objective of this article is comparison of surfaces with variable and constant depth microchannels with respect to boiling heat transfer enhancement, taking into account microchannels of 0.4 – 0.5 mm in wide.

2 Experimental setup

The diagram of the measurement stand for the determination of boiling curves is presented in Figure 1.

The main stand module (Fig. 2) consists of a vessel with four flat glass walls (2), filled with working fluid, and placed over the investigated sample (3). The sample was soldered to a 170 mm long cylindrical copper bar of 45 mm diameter. The cylinder diameter corresponded to the diagonal of the sample base. A 1000 W electric cartridge heater of 19 mm diameter and 130 mm long was installed into the bar. Before assembly the heater was coated with a special thermal paste to eliminate air spaces and decrease thermal resistance between the heater and cylinder material.

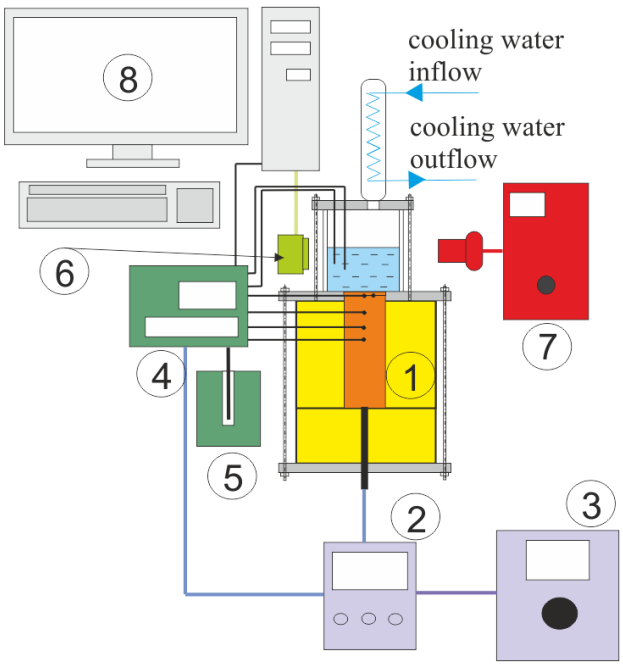

Fig. 1. Measurement system: 1 – main module, 2 – wattmeter, 3 – autotransformer, 4 – data logger , 5 – dry-well calibrator, 6 – high speed camera, 7 – lights, 8 – PC.

Type *K* (NiCr-NiAl) sheathed thermocouples of 0.5 mm in diameter were used for the measurements. They were placed as follows:

- in the liquid – saturation temperature measurement (*T1*, *T2*),
- under the sample – extrapolated to fin base temperature (*T3*, *T4*),
- in the bar at 5, 10, 20 and 35 mm depth (Fig .3) – temperature gradient determination (*T5*, *T6*, *T7*, *T8*).

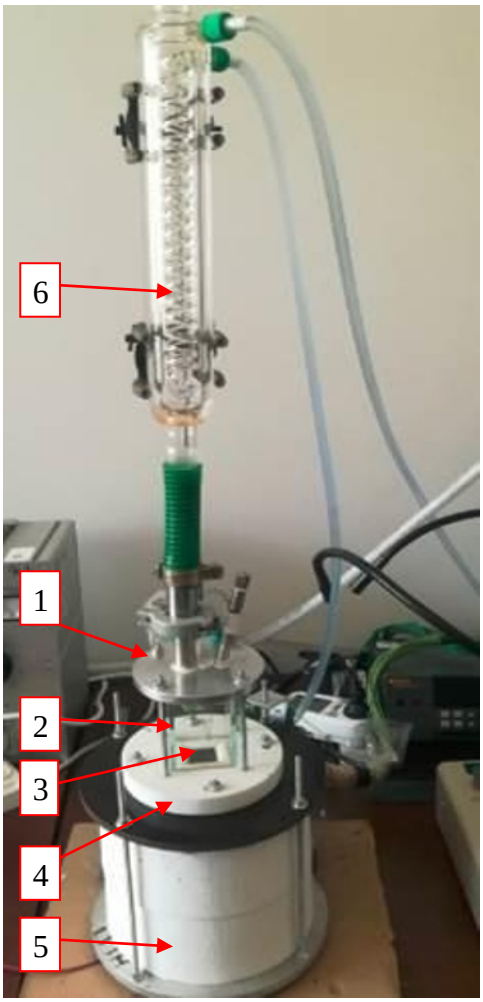

Fig. 2. Main module; 1 – top flange, 2 – glass vessel, 3 – sample, 4 – teflon annular flange, 5 – insulation, 6 – condenser.

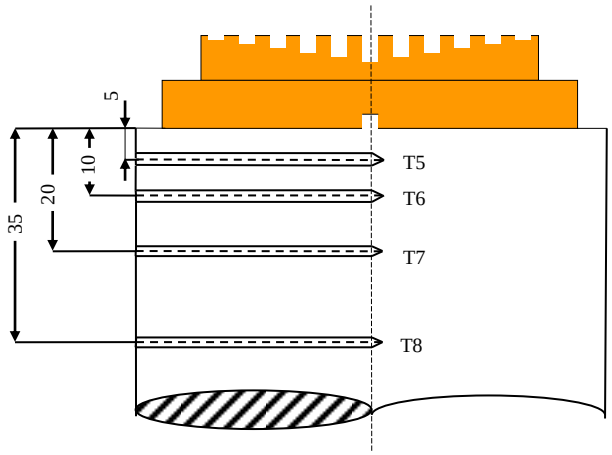

Fig. 3. Arrangement of thermocouples.

The heat flux was determined on the basis of the temperature gradient in the upper part of the heating cylinder, assuming one-dimensional heat conduction

$$q = \frac{\lambda_{Cu} \Delta T_{T5\text{-}T8}}{l_{T5\text{-}T8}} \quad (1)$$

Temperature superheat (ΔT) was related to micro-fin base. Due to the shift of the temperature measurement point, the superheat was calculated with the following dependence

$$\Delta T = \frac{T_{T3} + T_{T4}}{2} - \frac{q l_{T3,bs}}{\lambda_{Cu}} - T_{sat} \quad (2)$$

$l_{T3,bs}$ – means the distance between the microchannel top and thermocouples under the sample (*T3*,*T4*). The estimated uncertainties were as follows:

- low heat flux (2 kW/m^2): heat flux ±35%, heat transfer coefficient ±40%,
- high heat flux (550 kW/m^2): heat flux ±1.2%, heat transfer coefficient ±2.2%.

The method of Kline and McClintock was used to determine uncertainty. The quoted heat fluxes referred to the fin bases. The heat transfer coefficient was expressed as:

$$\alpha = \frac{q}{\Delta T} \quad (3)$$

3 Test surfaces

Original studies were conducted in order to plot boiling curves and perform visualisations on two types of structures (Figs. 4 and 5):

- with open microchannels of constant depth – MC
- with open microchannels of variable depth – MCV.

The samples with microchannels were made of copper and had parallel grooves with a constant pitch, made with an end mill (CNC machining process). The test section with a 27 x 27 mm^2 boiling region consisted of a 32 x 32 mm^2 base square copper sample.
Table 2 compiles the surface codes and specifications according to Figs 4 and 5.

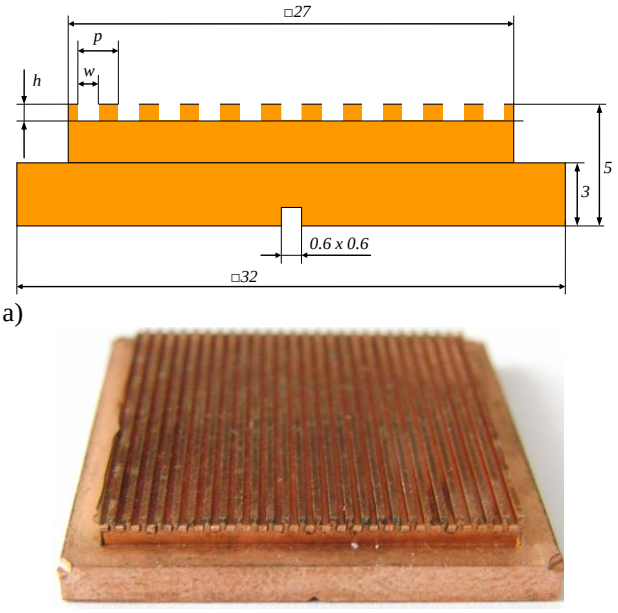

Fig. 4. a) Dimension symbols of the surface MC, b) view of the sample MC.

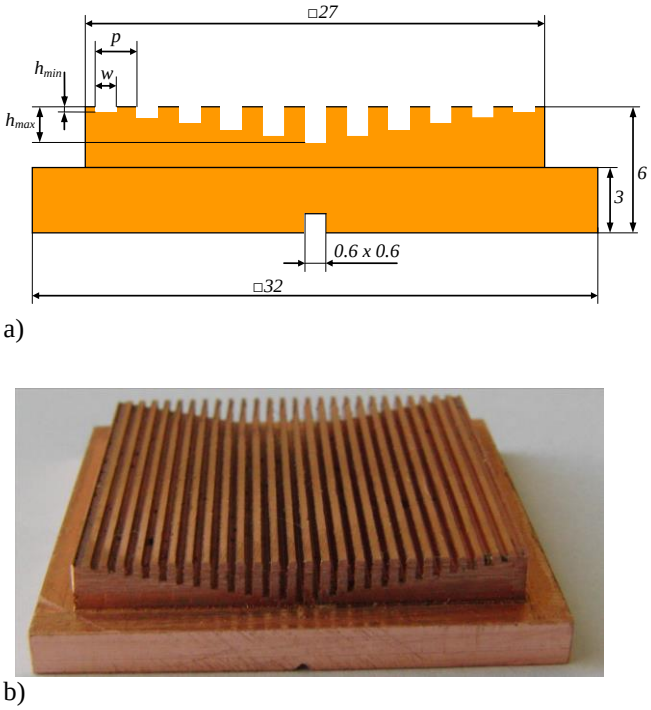

Fig. 5. a) Dimension symbols of the surface MCV, b) view of the sample MCV.

Table 2. MC/MCV surface codes and specifications.

Sample code	*w* mm	h_{min} mm	h_{max} mm	Δh mm	*p* mm
MC-0.4-0.5-0.8	0.4	0.5	0.5	0	0.8
MCV-0.5-0.2_2.8-1	0.5	0.2	2.8	0.2	1.0

4 Results

Two types of surfaces (MC and MCV) were examined to study the influence of the kind of extended surface on nucleate boiling heat transfer performance for two different liquids (water, ethanol).

The effect of the microchannel depth and width for water is shown in Fig. 6. The best results, with low and medium heat fluxes (q < 350 kW/m^2) were obtained for microchannels with variable depth (MCV). For higher heat fluxes microchannels with constant depth (MC) shows about 10% higher heat transfer coefficients than surface MCV. Boiling heat transfer enhancement for MCV related to plain surface (α/α_{ps}) is about 2 at heat fluxes 100 – 350 kW/m^2.

With ethanol boiling, the performance of microchannels has proved especially good for the MC surface (Fig. 7). Boiling heat transfer enhancement related to plain surface (α/α_{ps}) is 2 – 1.5 in the range q = 100 – 300 kW/m^2. Compared with MC surface, MCV surface gave lower heat transfer coefficients especially for higher heat fluxes (q > 300 kW/m^2).

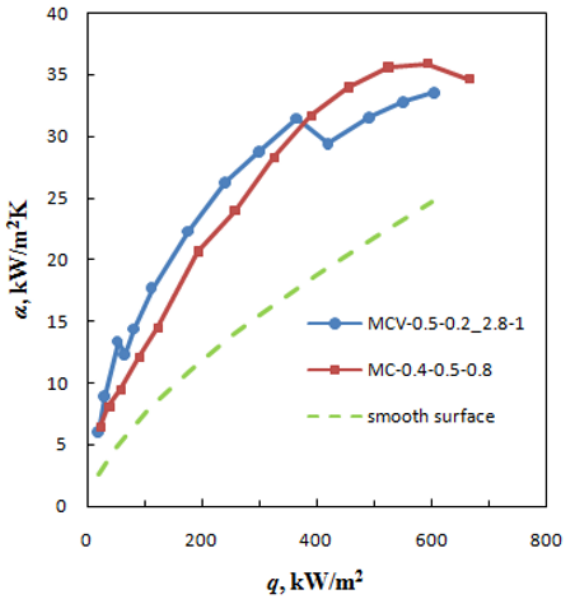

Fig. 6. Boiling curves for water, heat transfer coefficient vs. heat flux.

The mechanism of bubble nucleation, growing and departing is shown in Figs 8 and 9. Vapor bubble generated in microchannel spaces between neighboring microfins in the corner at the microchannel base. It grew and moved towards the microfin tip. The second stage of growth was observed when the bubble adhered to the top of the microfin. Increasing volume of the bubble increased buoyancy force. The growing bubble departed from the microfin top.

For microchannels of variable depth predicted boiling mechanism may be related to macroconvection with separate liquid-vapor pathways as well as with sustion-evaporation mode.

Figure 10 shows predicted boiling mechanism for microchannels with changing channels' depth. Small

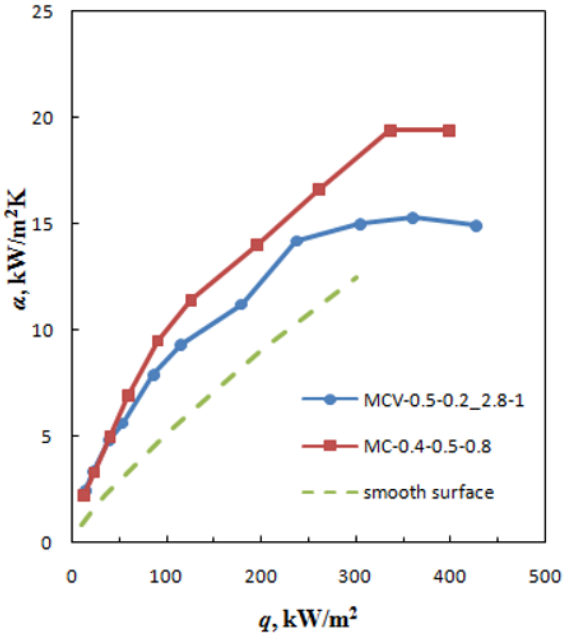

Fig. 7. Boiling curves for ethanol, heat transfer coefficient vs. heat flux.

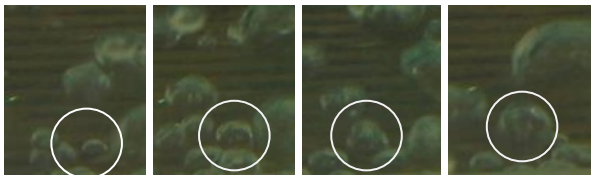

Fig. 8. Visualization observations of pool boiling of water on the microchannel surface MC-0.5-0.2_2.8-1, q = 30 kW/m^2, a) d=0.6 mm, b) d = 0.9 mm, c) d = 1.4 mm, d) d = 2.1 mm.

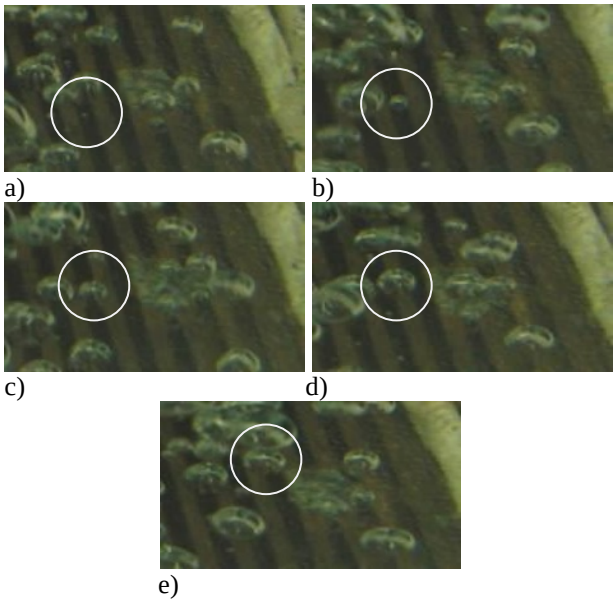

Fig. 9. Visualization observations of pool boiling of ethanol on the microchannel surface MCV-0.5-0.2_2.8-1, q = 30 kW/m^2, a) d = 0.25 mm, b) d = 0.5 mm, c) d =0.75 mm, d) d = 0.90 mm, e) d = 1.20 mm.

depth channels will contribute to the onset of nucleate boiling (ONB) at low superheating, but at medium heat flux heat transfer coefficient decreases after dry-out heat flux (DHF) is reached. Microchannels with greater depth improve the pool boiling performance at higher heat flux – they do not only provide an aditional surface for boiling heat transfer and nucleation, but they can prevent large bubbles from coalescing into a vapor blanket. This kind of vapor layer could cover the whole MC surface and ultimately dry out. Deep microchannels can eliminate this phenomenon, so that the critical heat flux (CHF) will have higher values.

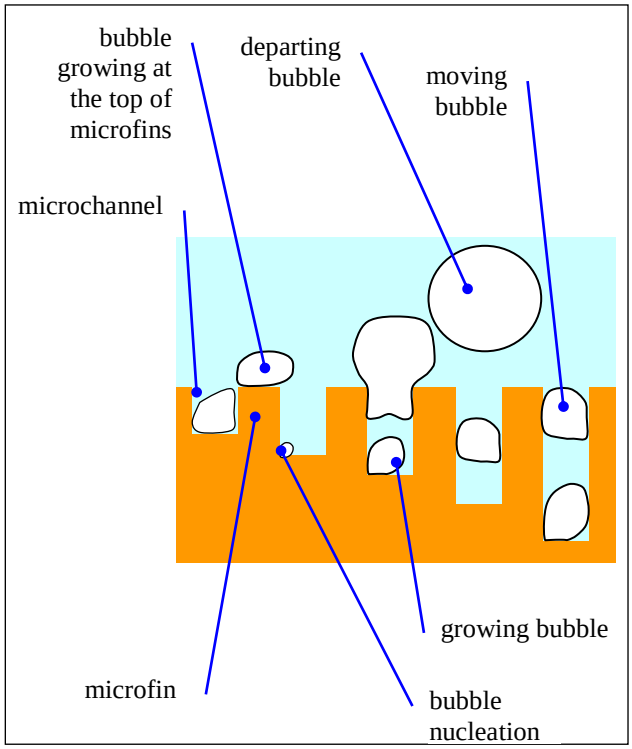

Fig. 10. Mixed boiling mode in microchannels of variable depth.

5 Conclusion

The following conclusions can be drawn from the experiments:

- When boiling water on microchannels with constant (MC) and variable depth (MCV), similar heat transfer coefficients (HTC) were obtained. During the boiling of ethanol, higher HTC values occurred at the highest heat fluxes.
- Visualization studies allowed the recognition of a two-stage bubble growing mechanism: initially at the bottom of the microchannel, and later at the top of the microfins that limit the microchannel.
- More exact conclusions can be drawn after testing a larger number of samples with MC and MCV surfaces in the range of 0.2 mm and 0.6 mm mm.

Nomenclature

CHF – critical heat flux,
d – diameter, m,
h – depth, m,
HTC – heat transfer coefficient,
l – distance between thermocouples, m,
MC – microchannel,
MCV – microchannel with variable depth,
p – pitch, m,
q – heat flux, kW/m^2,
T – temperature, K,
w – width, m,

Greek symbols

α – heat transfer coefficient, W/(m^{2}K),
λ – thermal conductivity, W/(mK),
Δh – change of depth, m,
ΔT – difference of temperature, K,

Subscripts

bs – base,
Cu – copper,
ps – plain surface,
sat – saturation,

References

1. D. Cooke, S. G. Kandlikar, J. Heat Transfer **133** (2011)
2. D. Cooke, S. G. Kandlikar, Int. J. Heat and Mass Transfer **55** (2012)
3. A. Jaikumar, S. G. Kandlikar, Int. J. Heat and Mass Transfer **95** (2016)
4. Ch. M. Patil, S. G. Kandlikar, Int. J. Heat and Mass Transfer **79** (2014)
5. A. Kalani, S.G. Kandlikar, proc. ASME 10th Int. Conf. Nanochannels, Microchannels and Minichannels, Rio Grande, Puerto Rico (2012)
6. A. Jaikumar, S. Kandlikar, Int. J. Heat and Mass Transfer **88** (2015)
7. A. Jaikumar, S. Kandlikar, App. Thermal Engineering **91** (2015)
8. A.M. Gheitaghy, A. Samimi, H. Saffari, App. Thermal Engineering **126** (2017)
9. R. Kaniowski, R. Pastuszko, Ł. Nowakowski, EPJ Web of Conferences **143**, 02049 (2017)
10. R. Kaniowski, R. Pastuszko, EPJ Web of Conferences **180**, 02042 (2018)
11. R. Kaniowski, R. Pastuszko, EPJ Web of Conferences **180**, 02041 (2018)
12. A. Kalani, S.G. Kandlikar, J. Heat Transfer. **135** (2013)
13. M.M. Rahman, M. McCarthy, J. Heat Transfer **139** (2017)
14. H. J. Kwak, J. H. Kim, B. Myung, M. H. Kim, D. E. Kim, Int. J. of Thermal Sciences **125** (2018)
15. A. Walunj, A. Sathyabhama, Appl. Therm. Eng. 128 (2018)